### Title
Regional differences in the response of California's rangeland production to climate and future projection




### Journal
Environmental Research Letters, 18(1)

### ISSN
1748-9318



### Authors
Liu, Han
Jin, Yufang
Roche, Leslie M
et al.



### Publication Date
2023

### DOI
10.1088/1748-9326/aca689

Peer reviewed

ENVIRONMENTAL RESEARCH
LETTERS

LETTER • OPEN ACCESS

# Regional differences in the response of California's rangeland production to climate and future projection

To cite this article: Han Liu *et al* 2023 *Environ. Res. Lett.* **18** 014011

IOP Publishing Environ. Res. Lett. 18 (2023) 014011 https://doi.org/10.1088/1748-9326/aca689

ENVIRONMENTAL RESEARCH
LETTERS



OPEN ACCESS

RECEIVED
7 October 2022

ACCEPTED FOR PUBLICATION
28 November 2022

PUBLISHED
19 December 2022



LETTER

# Regional differences in the response of California's rangeland production to climate and future projection

**Han Liu**[1,*], **Yufang Jin**[1], **Leslie M Roche**[2], **Anthony T O'Geen**[1] **and Randy A Dahlgren**[1]

[1] Department of Land, Air and Water Resources, University of California, Davis, CA, United States of America
[2] Department of Plant Science, University of California, Davis, CA, United States of America
[*] Author to whom any correspondence should be addressed.

**E-mail:** hanliu120@gmail.com

**Keywords:** ecosystem productivity, climate change, rangelands, remote sensing, Gradient Boosted Regression Trees, GCM, machine learning

Supplementary material for this article is available online

## Abstract

Rangelands support many important ecosystem services and are highly sensitive to climate change. Understanding temporal dynamics in rangeland gross primary production (GPP) and how it may change under projected future climate, including more frequent and severe droughts, is critical for ranching communities to cope with future changes. Herein, we examined how climate regulates the interannual variability of GPP in California's diverse annual rangeland, based on the contemporary records of satellite derived GPP at 500 m resolution since 2001. We built Gradient Boosted Regression Tree models for 23 ecoregion subsections, relating annual GPP with 30 climatic variables, to disentangle the partial dependence of GPP on each climate variable. The machine learning results showed that GPP was most sensitive to growing season (GS) precipitation, with a reduction in GPP up to 200 g $cm^{-2}$ $yr^{-1}$ when GS precipitation decreased from 400 to 100 mm $yr^{-1}$ in one of the driest subsections. We also found that years with more evenly distributed GS precipitation had higher GPP. Warmer winter minimum air temperature enhanced GPP in approximately two-thirds of the subsections. In contrast, average GS air temperatures showed a negative relationship with annual GPP. When the pre-trained models were forced by downscaled future climate projections, changes in the predicted rangeland productivity by mid- and end of century were more remarkable at the ecoregion subsection scale than at the state level. Our machine learning-based analysis highlights key regional differences in GPP vulnerability to climate and provides insights on the intertwining and potentially counteracting effects of seasonal temperature and precipitation regimes. This work demonstrates the potential of using remote sensing to enhance field-based rangeland monitoring and, combined with machine learning, to inform adaptive management and conservation within the context of weather extremes and climate change.

## 1. Background

Rangelands cover more than 30% of the global land area and are biologically diverse landscapes that include grasslands, shrublands, woodlands, wetlands, and deserts (Lund 2007). Changes in rangeland production affect many important ecosystem services, including carbon storage, nutrient cycling, water resource protection, biodiversity, and wildlife habitat (Li 2012, Roche *et al* 2015). Gross primary production (GPP) is a widely used metric for quantifying photosynthesis rate at the ecosystem scale. Recent studies have shown increasing interannual variability in GPP globally, with 57% of the variability contributed by rangeland-dominated ecosystems (Zhang *et al* 2016). In semi-arid rangelands, precipitation is, in most cases, the primary controller of GPP fluctuations (Jin and Goulden 2014, Zhang *et al* 2016). With projected increasing precipitation variability, the interannual variation in GPP is also predicted to increase (Zscheischler *et al* 2014). Therefore, monitoring GPP and understanding its variability may be a

useful benchmark indicator of ecosystem response to climate change.

In California, annual rangelands, which include open grasslands and woodlands dominated by an understory of herbaceous annual plants, are the primary forage source for the State's $3 billion livestock industry (California Department of Food & Agriculture 2015). These annual rangelands comprise approximately 4 million hectares, encompassing portions of the Central Valley, the Coast Ranges and Sierra Foothill Region (FRAP 2017). California rangelands are highly variable, in part, because the plant community phenology, consisting of annual grasses and forbs, is dynamically linked to seasonal weather patterns (Stromberg *et al* 2007). For example, the growing season (GS) is initialized by fall rains (September–December) exceeding 1.25–2.5 cm during a seven-day period, which promotes germination. Plant growth is slow in winter (December–February), due to low air temperatures and low solar radiation. In late winter/early spring (February–April), rapid growth begins as air temperature increases (>7.2 °C) and solar radiation intensifies. Finally, in mid-late spring (April–June), plant production reaches peak biomass once root zone moisture is depleted. Thus, California rangeland GPP varies significantly seasonally and from year-to-year (Jin and Goulden 2014), in response to short-term changes in climate and solar radiation. The large gradient of topography and long term climate across California's diverse landscape also shapes the spatial patterns of rangeland GPP (Liu *et al* 2021) and potentially a differentiating sensitivity to climate change.

Over the past decades, researchers have relied on regression and/or correlation analyses to examine drivers regulating variability in annual GPP and plant biomass production on rangelands at different scales. Taking advantage of the high correlation between absorbed photosynthetically active radiation and GPP, Jin and Goulden (2014), for example, reported GPP was positively related to annual precipitation, with higher sensitivity in grasslands than woody shrublands in California. A few other studies also reported positive response of rangeland GPP to annual precipitation amount in Northern China (Guo *et al* 2015), North America (Wu and Chen 2012), and across the entire globe (Huang *et al* 2016).

Annual GPP can be further regulated by other climate variables. Seasonal distribution of rainfall events has a significant impact on rangeland GPP by regulating the active GS (Xu and Baldocchi 2004). Warming air temperature was found to reduce GPP in northern Eurasia's southwestern grasslands, although it was the primary reason for recent GPP increases in northern Eurasia's shrublands (Dass *et al* 2016). In California, rangeland production is predicted to increase as air temperatures become warmer in the San Francisco Bay Area as early as mid-century (Chaplin-Kramer and George 2013); however, another study predicted a 14%–58% decrease in rangeland production across California using a precipitation-based model (Shaw *et al* 2011). Previous small scale studies showed that variations in GPP were related to the combined effects of various climatic variables, and the relationship between GPP and climatic variables may vary across different locations. Thus, to fully understand variations in GPP and predict future changes, it is necessary to build individual models with respect to different regions and consider a suite of relevant climate variables, including precipitation amount, seasonal precipitation distribution, air temperature, and solar radiation.

A long-term record of annual GPP at moderate resolution is critical for a more robust analysis of interannual variability in GPP and for building data-driven models. Advances in both remote sensing technologies and data analysis are providing novel, cost-effective opportunities to obtain data at management-relevant scales for terrestrial-ecosystem research, which has otherwise relied on traditional statistical methods and field-based monitoring that require substantial time and labor resources (Briske *et al* 2017). The Moderate Resolution Imaging Spectroradiometer (MODIS) has been collecting terrestrial observations for more than 20 years on a daily basis since the launch of Terra satellite in 1999 (Savtchenko *et al* 2004). GPP products derived from MODIS satellite images at 500 m spatial resolution are available at an eight-day interval for the entire globe (Running *et al* 2019). Machine learning models have also become more interpretable while keeping the powerful non-linear, multi-parameter model fitting functionalities (Molnar 2019). These advances are key because traditional statistical models lack the ability to disentangle the interactions among variables (Lee *et al* 2020, Liu *et al* 2021).

In this study, we aimed to improve our understanding of temporal variability in rangeland annual GPP and assess how its sensitivity to changes in weather and climate may vary across different ecoregions in California. The machine learning models were built to learn the complex climate impacts on GPP, by leveraging 20 years of contemporary records on weather and remote sensing based GPP. Using the developed models, we further predicted and evaluated how rangeland annual GPP would change under different climate projections by mid and end of century over California's diverse landscape. We hypothesized that the primary climatic variable regulating California annual rangeland GPP varies by regions. This spatial variability results from the influence of other climatic and environmental variables that become more pronounced as precipitation increases, especially when water is no longer the primary limiting resource.

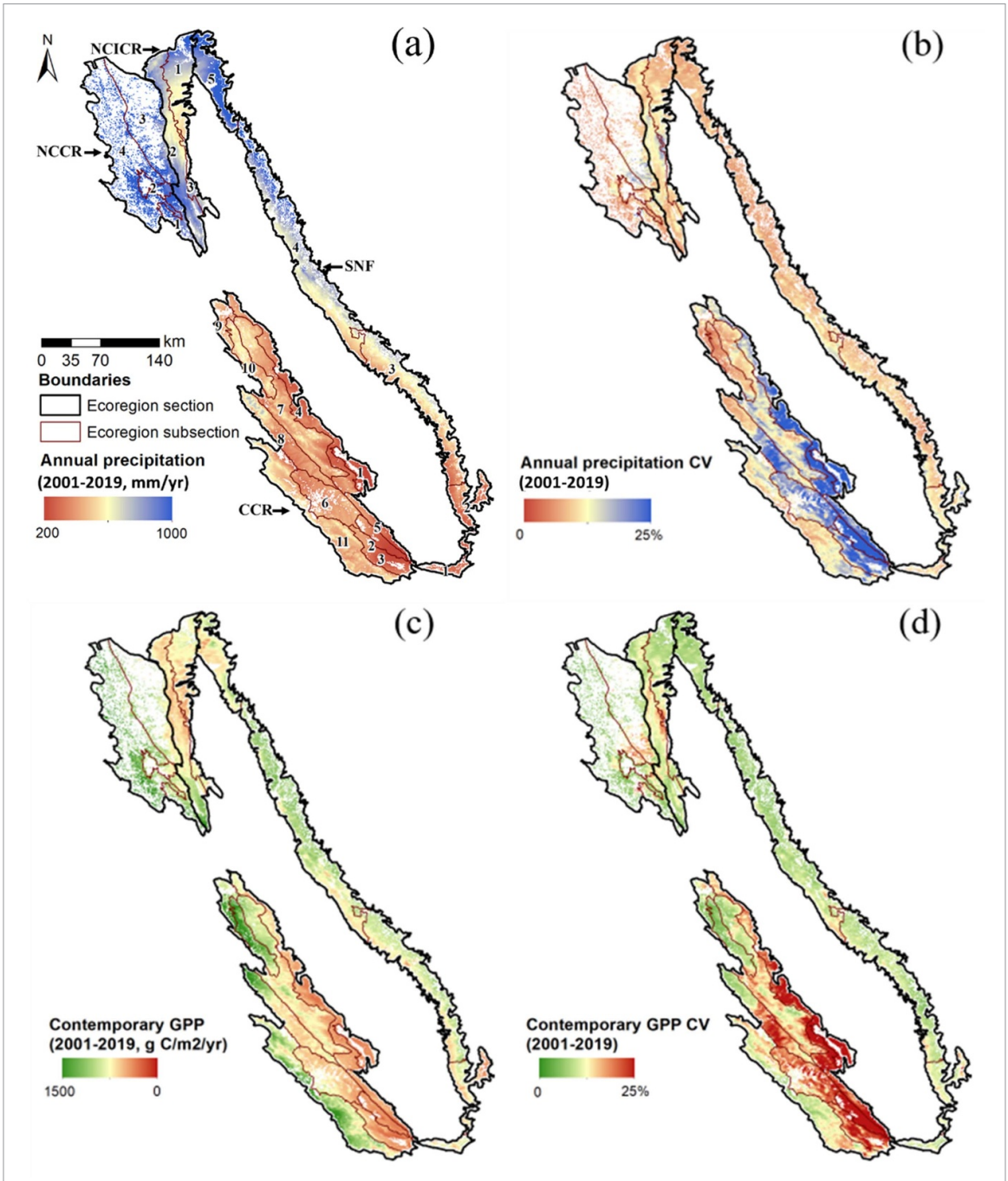


**Figure 1.** Statewide distribution of long-term-mean (a) precipitation and (c) GPP during 2001–2019 over California's annual rangelands. Maps of year-to-year variability in precipitation (b) and GPP (d) as quantified by the coefficient of variation. The study area encompasses four ecoregions (black lines) that are further divided into 23 subsections (orange lines).

## 2. Data & methods

### 2.1. Study area

Our study focused on California annual rangelands, spanning 33°–41° N and 118°–124° W, with a wide range of microclimates resulting from complex geographic and topographic diversity. The study area encompasses four major ecoregions as delineated by the Ecological Classification and Mapping Task Team (Cleland *et al* 2007): Northern California Coast Ranges (NCCR), Northern California Interior Coast Ranges (NCICR), Central Coast Ranges (CCR), and Sierra Nevada Foothills (SNF) (figure 1(a)). Annual rangelands feature a Mediterranean climate with hot, dry summers and mild, moderately wet winters. The active GS of annual rangelands coincides with the rainy season: germination typically ensues in late fall (November), and senescence occurs after the rainy season ceases in late spring or early summer (April–May).

Precipitation varies considerably across ecoregions, with long-term-means (LTMs) ranging from 160 mm $yr^{-1}$ in the CCR to 2290 mm $yr^{-1}$ in the NCCR (figure 1(a)). Coastal regions are relatively cooler in the summer and receive higher amounts of precipitation than inland regions, especially those in

rain shadows. Across the study area, air temperature increased from the coast to inland, north to south, and from valleys to mountains. Due to the significant heterogeneity of the landscape, the four major ecoregions are further divided into 23 ecoregion subsections based on similar ecological potentials, determined by many biotic and environmental factors such as climate, physiography, soils, hydrology, and potential natural communities (figure 1(a)) (Cleland *et al* 2007). We hereafter refer to ecoregion subsections by their parent ecoregion abbreviation followed by a unique number as specified in figure 1(a).

### 2.2. Contemporary satellite and climate data

We obtained the version 6 gap-filled GPP product (MYD17A2HGF) at 500 m resolution every eight days from MODIS Terra and Aqua during 2000–2019 (https://earthdata.nasa.gov/). MODIS provides frequent multispectral moderate-resolution (250–500 m) observations, revisiting the globe once to twice per day since 2000. We calculated water year (October–September) (U.S.Geological Survey 2016) cumulative GPP from the 8 day product (Running *et al* 2019). A LTM annual GPP layer ($820 \pm 283$ g cm$^{-2}$ yr$^{-1}$) was derived from 2001–2019 as a measure of spatial variation in forage production (figure 1(c)). Annual rangeland GPP varied significantly from year to year as shown in figure 1(d), with a statewide mean ranging from 1017 g cm$^{-2}$ yr$^{-1}$ in 2005–750 g cm$^{-2}$ yr$^{-1}$ in 2008 (see detailed discussion in supplemental materials section 1).

Meteorological data during 1986–2019 came from Daymet hosted at the Oak Ridge National Laboratory Distributed Active Archive Center (Thornton *et al* 2016). The gridded daily surface weather parameters at a 1 km resolution were interpolated from more than 8000 meteorological stations, based on a digital elevation model (Thornton *et al* 2016). We aggregated daily precipitation, min/max/mean air temperatures, and solar radiation to monthly and seasonal averages, resulting in a total of 30 climatic variables to be explored (as detailed in table S1). To quantify seasonal precipitation variation between the driest and wettest months during the GS, a Precipitation Concentration Index (PCI) was calculated as the ratio of the sum of squares of the wet season monthly precipitation (November–May) over squared water year precipitation multiplied by a scaling factor of 58 (Oliver 1980, Sloat *et al* 2018).

### 2.3. Future climate projection data

For future climate, we obtained daily climate projections downscaled for California from Cal-Adapt Data Server (http://albers.cnr.berkeley.edu/data/scripps/loca/). This dataset is bias-corrected and downscaled to a resolution of 1/16° (~6 km) from 32 global climate models (GCM) using the localized constructed analogues statistical method (Pierce *et al* 2018). The data include both the historical simulations during 1950–2005 and future climate projections during 2006–2099 under two emission scenarios that have been widely used (e.g. by the California's climate change assessments) for climate related policy decisions (IPCC 2013). Representative Concentration Pathway (RCP) 4.5 (Thomson *et al* 2011) is an intermediate scenario where greenhouse gas emissions peak around 2040 and then decline (IPCC 2013). A worst-case scenario, RCP 8.5, represents rising emissions throughout the 21st century (Thorne *et al* 2017). In this study, we used projections from four GCMs that have demonstrated good performance in reproducing California's historical climate (Pierce *et al* 2018): HadGEM2-ES, MIROC5, CNRM-CM5, and CanESM2.

For each model and scenario projection, we acquired daily mean precipitation, air temperature (minimum, maximum, and mean), and solar radiation layers. To match the contemporary record, a bias adjustment was applied to the GCM data, based on 20 years of overlapping time periods between Daymet and GCM historical simulations. We first calculated the differences between Daymet and GCM data derived for each climate variable (see table S1) for each overlapping year during 1986–2005. LTM offsets were then calculated, and applied to the original GCM projection to derive bias-adjusted future climate data.

### 2.4. Machine learning GPP model development

Using the contemporary records of satellite derived GPP and Daymet weather during 2000–2019, we built Gradient Boosted Regression Trees (GBRT) models for each ecoregion subsection to investigate the complex associations between the interannual variability in annual rangeland GPP and climatic drivers. The annual GPP layers were resampled to 1-km resolution with a linear method to match the Daymet grid size. The LTM GPP at 1 km was included as an additional independent variable (table S2: LTMGPP, top one or two variables), in order to account for spatial variability in GPP caused by topography and soils.

GBRT is one of the most popular ensemble machine learning methods that combine outputs from many individual trees to overcome the potential poor performance and reduce the risk of overfitting faced by single learner methods (Friedman 2001). Instead of building trees independently, it fits regression trees sequentially, with each tree aimed at minimizing prediction residuals of its predecessors (Friedman 2001). GBRT is a powerful tool for discovering and representing nonlinearities and complex interactions among predictors (Elith *et al* 2008), because the hierarchical tree structure inherently models the dependence of the response variable to one predictor given the values of inputs higher in the tree. For each ecoregion subsection, a GBRT model was trained with 70% randomly selected pixel-years, using key variables selected from table S1.

Feature selection was conducted to remove redundant climatic variables and reduce potential overfitting issues. We first iteratively eliminated variables with respect to their correlation to other variables (i.e. when two variables are highly correlated ($r > 0.8$), removing the variable having the lower distance correlation (Székely *et al* 2007) with annual rangeland GPP. We further removed variables that had low predictive power using the Recursive Feature Elimination with cross-validation technique (Guyon *et al* 2002). Finally, a permutation importance-based feature selection was performed to further reduce the number of variables. Permutation importance is computed as a decrease in the model performance (for example, measured by $R^2$ or Root Mean Squared Error (RMSE)) when a variable is permuted. We sequentially permuted variables with the least permutation importance score and fitted models with the most important three to nine variables. For the purpose of balancing model accuracy and complexity, we kept the top seven variables to build ecoregion subsection-specific machine learning models (figure S1).

We investigated how each of the key climatic variables affects interannual rangeland GPP variation using partial dependence plots from the GBRT models (Friedman 2001, Friedman and Meulman 2003). Partial dependence function shows the response to one target predictor after accounting for the average effects from all other predictors, by marginalizing the model over the distribution of other independent variables (Molnar 2019). It is therefore used here to visualize and disentangle the interactive response of GPP to a suite of climate variables. The *y*-axis of partial dependence plots represents the difference between the marginalized prediction and mean GPP for each value of the predictor on the *x*-axis. For example, a wide range on the *y*-axis indicates strong sensitivity of GPP to the target predictor when other confounding factors are excluded.

### 2.5. Future GPP projection and attribution

To predict future rangeland GPP, we applied the trained GBRT models, built specifically for each ecoregion-subsection, to bias-adjusted climate projections from 2040–2099 as described in 2.3. For a consistent comparison, GPP estimations by the same models driven by the Daymet climate data during 2001–2019 were used as a contemporary baseline. The results were summarized by taking the means over three-time windows: contemporary (2001–2019), mid-century (2041–2059), and end of century (2081–2099), under two emission scenarios.

We further quantified changes in GPP by mid-century and end of the century caused by each type of climatic variable (e.g. precipitation amount, precipitation distribution, minimum air temperature, mean air temperature, maximum air temperature, and solar radiation). For each type of variable, the attribution was performed by comparing the difference between GPPs predicted for the contemporary period and GPPs predicted with the future climate simulation for the target type of variables while keeping all other variables as the contemporary climate. Differences between this newly predicted GPP and the original contemporary GPP indicate the extent to which changes in GPP are attributed to changes in precipitation, air temperature, and solar radiation.

## 3. Results

### 3.1. Sensitivity of interannual rangeland GPP to climate

For each of the 23 subsections, we chose the top seven climate variables (see table S2) to model annual rangeland productivity at 6-km, based on GBRT model-based feature selection as detailed in section 2.3. Predicted GPP was shown in good agreement with the MODIS GPP product when tested against the validation dataset, with an $R^2$ of 0.97, RMSE of 30.7 g $cm^{-2}$ $yr^{-1}$, and a mean absolute percentage error of 4.1% (figure S2).

Overall, precipitation-related variables were found important for 23 subsections for capturing interannual variation in rangeland productivity (table S2 and figure 2). Specifically, at least one variable representing precipitation amount was selected for all subsections, either for individual winter and/or spring months or seasonal cumulative amount, depending on the region (figure 2(a) and table S2). Over eight subsections, precipitation amount during the GS enhanced annual GPP before reaching a plateau at 300–700 mm $yr^{-1}$, depending on the subsection (figure 3(c)); production in the drier subsections of the central coast were most sensitive, with a decrease by more than 200 g $cm^{-2}$ $yr^{-1}$ when GS precipitation varied from 400 to 100 mm $yr^{-1}$.

PCI was critical in 21 subsections, except for the two driest subsections on the central coast. Partial dependence plots from subsection-specific GBRT models showed that annual GPP decreased rapidly before the curves flattened at a PCI equal to 13 (figure 3(a)). This suggests that years with more evenly distributed precipitation (i.e. lower PCI values) had higher GPP than years with less evenly distributed precipitation (i.e. higher PCI values), when everything else was held constant.

Winter monthly minimum air temperature (November–February), was the third important variable category, followed by mean air temperature, selected by 19 and 9 subsections, respectively (figure 2). $T_{max}$ and solar radiation during GS were important in less than five subsections, mostly in north coast interior and central coast (table S2).

Air temperatures ($T_{min}$, $T_{mean}$, and $T_{max}$) showed different controls on GPP. Warmer January minimum air temperature enhanced annual GPP as it warmed from 0 °C to 6 °C (figure 3(b)). In contrast,

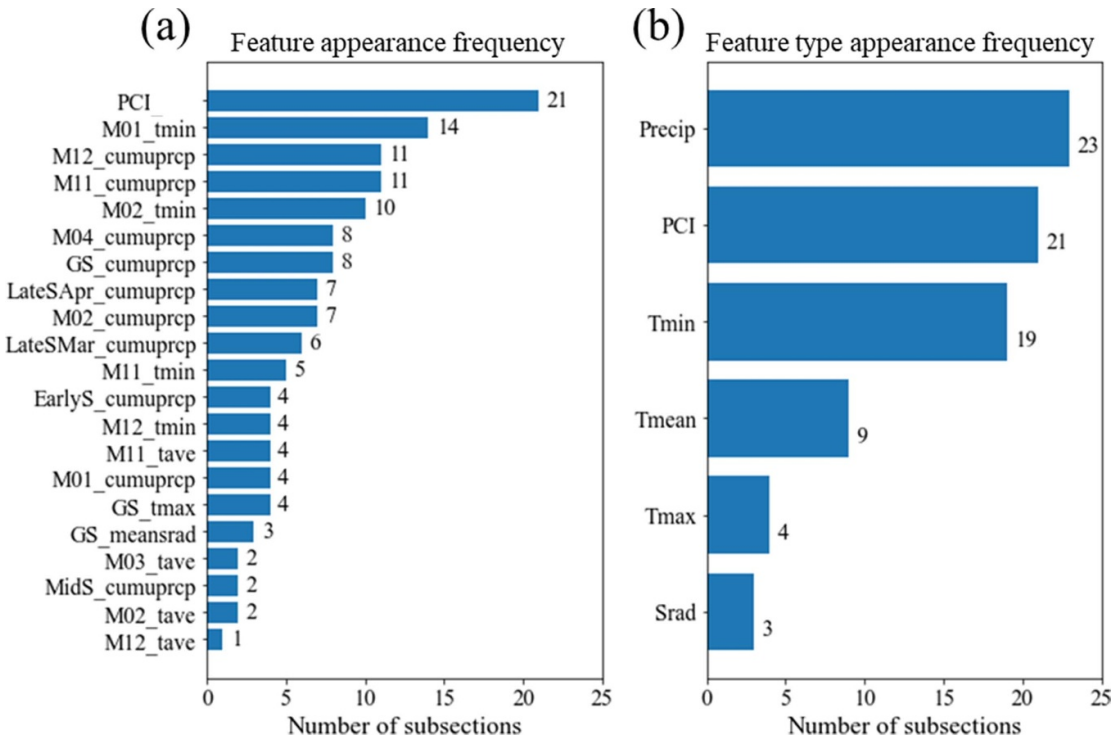


**Figure 2.** Prevalence of selected (a) climate variables and (b) climate variable groups, summarized among the 23-subsection specific models. For example, an appearance in 21 subsections for the precipitation concentration index (PCI) was selected as one of the seven top variables in 21 subsection models. Tmin, tave/tmean, and tmax stand for minimum, average, and maximum air temperature. Cumuprcp stands for cumulative precipitation. Srad stands for shortwave solar radiation. See table S1 for a full list of variable abbreviation definitions.

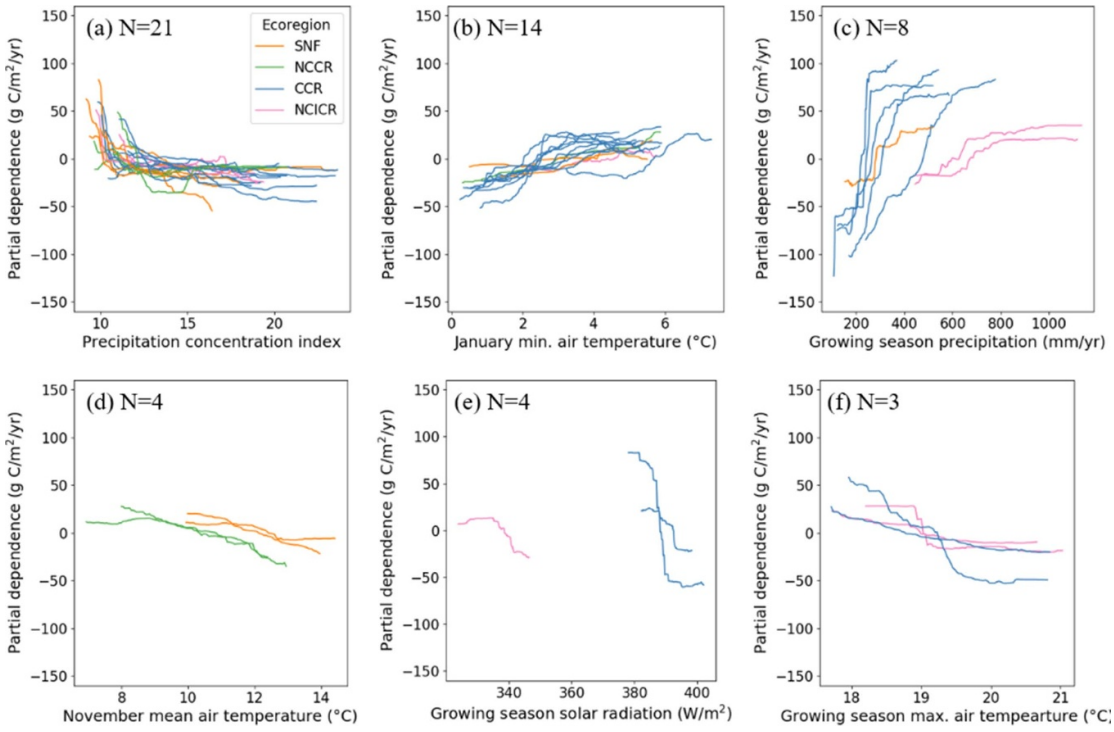


**Figure 3.** Partial dependence of annual GPP on selected key climate variables, including (a) precipitation concentration index (PCI), (b) January minimum air temperature, (c) (growing season (GS), October–May) precipitation amount, (d) November mean air temperature, (e) GS solar radiation, (f) GS maximum air temperature.

mean November air temperature and GS maximum air temperature showed a negative impact on annual GPP (figures 3(d)–(f)). For example, as November mean air temperature increased from 7 °C to 14 °C, GPP decreased from 10∼40 g $cm^{-2}$ $yr^{-1}$ above the LTM (during 2001–2019) to 5∼40 g $cm^{-2}$ $yr^{-1}$ below

**Table 1.** Projected GPP (g cm$^{-2}$ yr$^{-1}$) for the entire study area (lower and upper 25% quantiles, mean and standard deviation) during contemporary (2001–19), mid-century (2041–59), and end of century (2081–99) periods under two different emission scenarios, as compared to the contemporary time period. Results summarized from the predicted GPP ensemble at 6 km by machine learning models driven by future climate projections from four GCMs. Areas are expressed as percentage of the entire study area.

| | RCP4.5 | | | RCP8.5 | | | | RCP4.5 | | RCP8.5 | |
|---|---|---|---|---|---|---|---|---|---|---|---|
| | Q25 | Mean± Std | Q75 | Q25 | Mean ± Std | Q75 | | Area | Mean changes ± Std | Area | Mean changes ± Std |
| Contemporary (2001–2019) | 663 | 816 ± 271 | 973 | — | — | — | — | — | — | — | — |
| Mid-century (2040–2069) | 643 | 809 ± 260 | 947 | 647 | 812 ± 258 | 942 | Increased GPP | 40% | 17 ± 16 | 44% | 18 ± 15 |
| | | | | | | | Reduced GPP | 60% | −17 ± 14 | 56% | −19 ± 21 |
| End of century (2070–2099) | 639 | 812 ± 264 | 959 | 642 | 813 ± 265 | 959 | Increased GPP | 41% | 23 ± 18 | 53% | 27 ± *18* |
| | | | | | | | Reduced GPP | 59% | −27 ± 21 | 47% | −37 ± *32* |

the LTM in subsections SNF-3, SNF-4, NCCR-3, and NCCR-4 (figure 3(d)). Maximum air temperature during the GS showed a more substantial negative impact than mean air temperature. Annual GPP decreased more than 100 g cm$^{-2}$ yr$^{-1}$ as GS maximum air temperature increased from 17 °C in a colder year to 21 °C in a warmer year in CCR-2, CCR-3, NCICR-1, and NCICR-3 (figure 3(f)). Despite the large latitudinal difference, all subsections had higher annual GPP in years with a lower amount of solar radiation (figure 3(e)).

### 3.2. Changes in GPP under future climate projections

When driven by future climate projections from four GCMs, the GBRT model predictions showed that, cross the entire study area, mean annual GPP was projected to decrease from 816 ± 271 g cm$^{-2}$ yr$^{-1}$ to 809 ± 260 g cm$^{-2}$ yr$^{-1}$ by mid-century and to 812 ± 264 g cm$^{-2}$ yr$^{-1}$ by the end of the century (2081–2099) under RCP4.5 (table 1). Although mean reductions in GPP were projected to be small, these changes were not spatially uniform within the study area (figures 4 and 5). Both the lower and upper quantiles of the predicted mid-century GPP showed more significant reductions (e.g. by 20 and 26 g cm$^{-2}$ yr$^{-1}$, respectively). Predicted GPP decreased in over 59% of the study area by 27 ± 21 g c m$^{-2}$ yr$^{-1}$ by the end of the century, which was partly counteracted by an increase over 41% of the study area (23 ± 18 g cm$^{-2}$ yr$^{-1}$) compared to the contemporary period (2001–2019) (table 1).

Under the RCP8.5 emission scenario, the model predicted GPP changes similar to the RCP4.5 model over our study area; however, compared to the RCP4.5 model, a smaller extent of the study area would exhibit GPP reductions (i.e. only 56% and 47% by mid- and end of century, respectively) (table 1). The magnitude of changes in GPP was larger though than under RCP4.5, especially by the end of the century, i.e. by −37 ± 32 g cm$^{-2}$ yr$^{-1}$ (table 1).

### 3.3. Spatial patterns of future GPP change and climate change contributions

Future GPP reductions were predicted to occur mostly in moderate to wetter areas, such as NCCR, central and southern Sierra Nevada, relatively wetter parts of the Central Coast, and to a lesser degree in NCICR (figures 5 and 6(a)). Less evenly distributed precipitation during the rangeland GS, as indicated by the projected increase in PCI (Figures. S4c and S5c), contributed the most to the GPP decrease by both mid- and end of the century, especially over regions with intermediate rainfall (figure 6(b)). For example, GPP declined by as much as 15–30 g cm$^{-2}$ yr$^{-1}$ in subsections CCR-11, SNF-3, and SNF-4 (more than 29% of the entire study area) where the impact of PCI was dominant. In wetter regions, reduction in GPP was further caused by warmer $T_{mean}$ during GS such as in CCR and SNF (figures S4(e) and S5(e)). Warmer Feburary $T_{min}$ (figures S4(d) and S5(d)) was also predicted to induce a GPP reduction in costal subsections NCCR-1 and CCR-11, except in the wettest costal subsection NCCR-4.

In contrast, increases in predicted future GPP were found mostly in drier and less productive subsections, as shown in the 6 km map (figure 5) and summarized at the ecoregion subsection level (left-hand side of figures S4–S6), with a few exceptions. GPP in drier subsections that received less than 513∼522 mm yr$^{-1}$ precipitation, mostly in the CCR, benefited from a predicted increase in precipitation (figure S4(b)). Increasing minimum air temperature (figures S4(d) and S5(d)) further enhances rangeland productivity in these areas (figure 6). The projected increase in maximum air temperature under RCP 4.5,

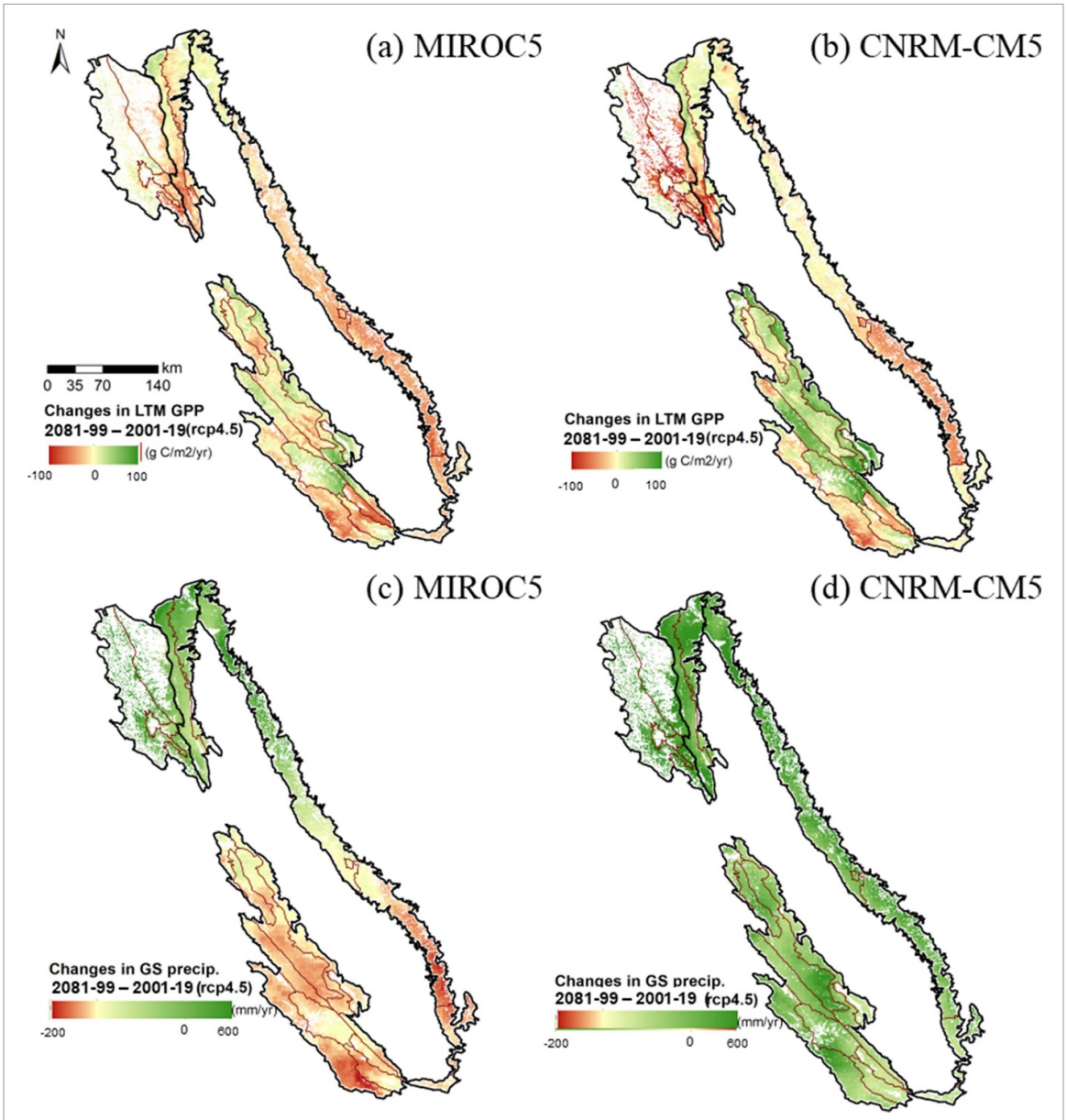


**Figure 4.** Predicted changes in GPP based on (a) MIROC5 (dry model) and (b) CNRM-CM5 (wet model), as well as the corresponding simulated changes in GS precipitation (c), (d) by the end of century under the intermediate scenario (RCP4.5).

however, caused a significant decline in GPP in the southern drier end of the central coast and northern interior coast, by 45 and 12 g $cm^{-2}$ $yr^{-1}$ in CCR-2 and CCR-3, and 13 g $cm^{-2}$ $yr^{-1}$ in NCICR-3, respectively.

## 4. Discussion

### 4.1. Impacts of climate variables on rangeland GPP

This study leveraged 20 years of remote sensing records and machine learning methods to quantify and disentangle the interactive response of annual GPP to a suite of climate variables across California's annual rangelands. We found a high degree of spatial variability in responses across the 23 ecologically distinct subsections, as a result of varying sensitivity to climate change. While the relative importance of climatic variables varied in controlling interannual GPP variability across ecoregion subsections, variables related to precipitation, in general, were major drivers of rangeland productivity responses. Moving from drier to wetter areas, the driving climatic variable for GPP shifted from total GS precipitation to the relative distribution of GS rainfall (PCI). This is consistent with previous findings from field observations—that is, water is likely no longer the limiting factor to plant growth in wet regions in most years. Instead, timing and monthly distribution of precipitation become more important because, as intervals between rainfall events increase, the duration and severity of soil water stress is expected to increase (Knapp *et al* 2008). Furthermore, we found greater total precipitation in wetter areas reduced GPP, likely in part because oversaturated soils can create anaerobic conditions that impair growth and development of upland (i.e. non-wetland species) plants (Wilson and Livingston 1932). Wetter years

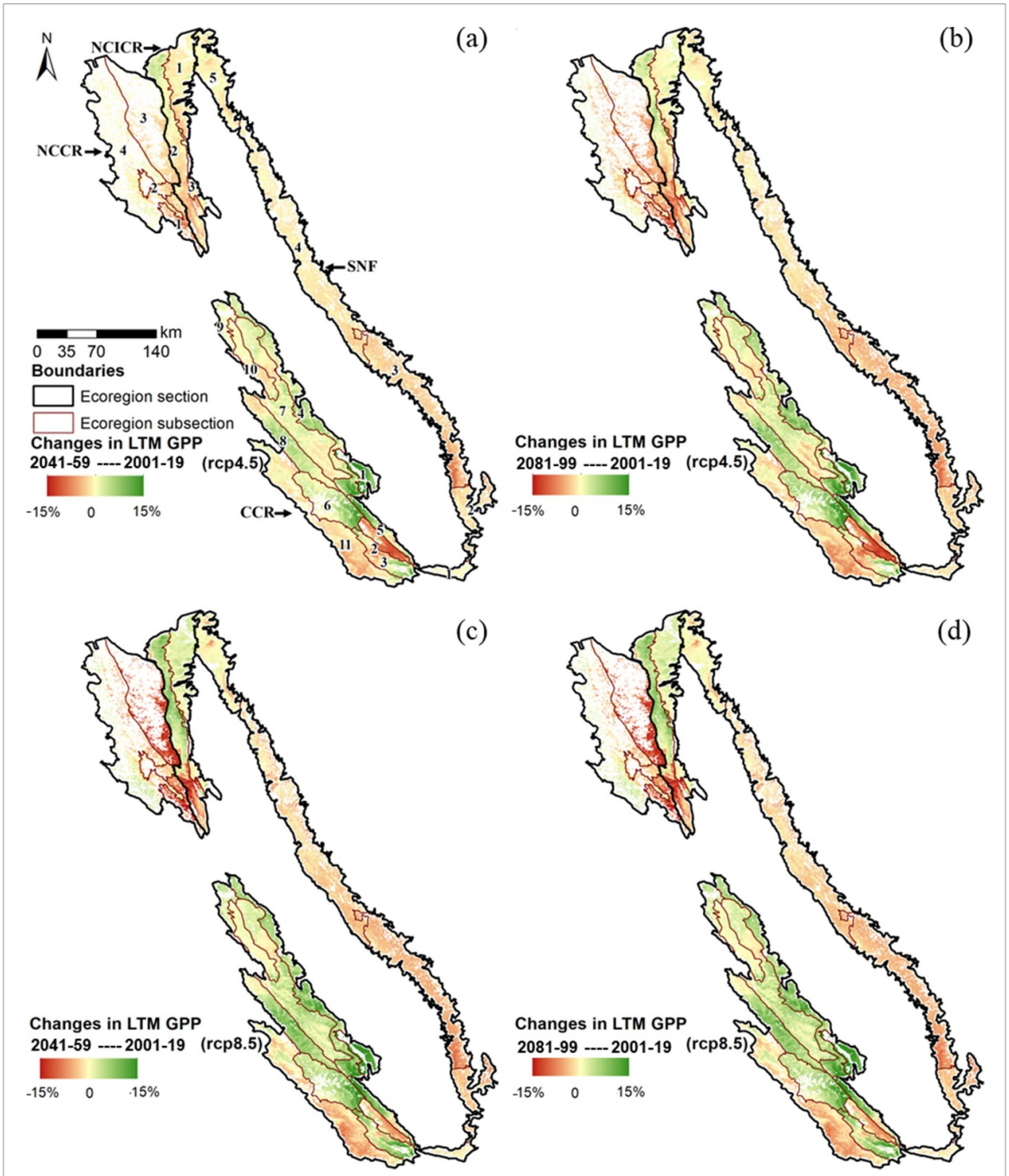


**Figure 5.** Percentage change in mean predicted GPP due to climate changes projected by four GCMs by (a), (c) mid-century and end of century (b), (d) compared to the contemporary period under (a), (b) intermediate (RCP4.5) and (c), (d) worst-case (RCP8.5) scenarios.

may also have colder temperatures and lower solar radiation resulting from greater cloud cover.

Air temperatures (minimum, mean, and maximum) showed different controls on GPP. We found a positive relationship between GPP and winter minimum air temperature in all but four subsections (SNF-1, SNF-2, SNF-3, and NCCR-3), likely due to warmer temperatures in the early season promoting germination and early growth (Becchetti *et al* 2016). In contrast, Mean and maximum air temperatures had a negative control on GPP in several subsections across the study area, likely by increasing water demand and thus causing water stress (Devine *et al* 2019). Higher solar radiation during GS was also shown to cause GPP reduction in three subsections, probably via enhanced drying processes. Further work is needed to better understand coupling effects of climate variables, such as the combined impacts of cold temperatures and high precipitation on GPP, as well as reasons for spatial differences in climate controls on GPP, such as why GPP is not as responsive to air temperature in some areas as it is in other areas.

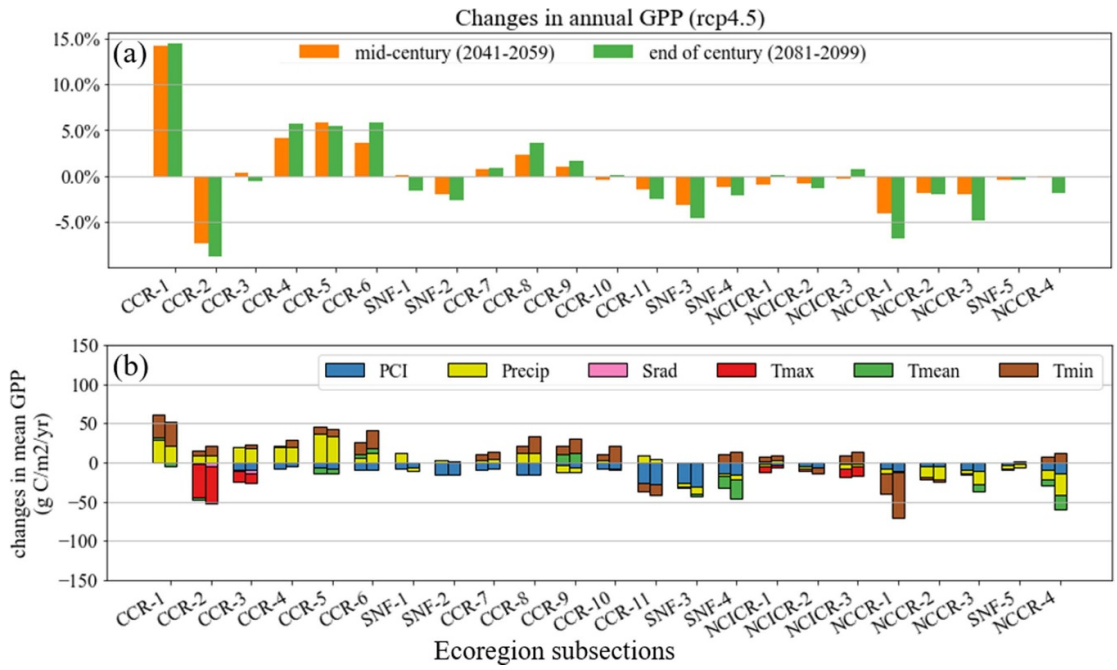


**Figure 6.** Percent change in GPP and their attribution to climatic variables for the 23 subsections under the intermediate scenario (RCP4.5). Subsections are ordered from driest (left) to wettest (right). For attribution under RCP8.5, see figure S6.

### 4.2. Implications of future changes in rangeland GPP

While our models predicted small changes in future rangeland productivity for the study area as a whole (table 1), impacts at the ecoregion subsection scale were more marked and suggest rangeland productivity responses to climate change will be highly variable at the local level (figure 4). We found greater magnitude of GPP changes (mostly increases) in many drier subsections (figure 6(a)) in response to slightly higher predicted precipitation and higher GS minimum temperatures over time. Considering the entire study area, predicted increases in GPP from favorable future precipitation and temperature conditions in mostly drier subsections (41% of the study area) were counterbalanced by predicted decreases in GPP from unfavorable changes in temperature, rainfall distribution, and solar radiation in wetter subsections (59% of the study area)—resulting in the overall small decrease in GPP.

However, it is worth noting that several uncertainties in GPP projections exist due to inconsistencies among GCMs, especially in precipitation simulations. For example, although four GCM projections agreed on larger variation in monthly precipitation (less evenly distributed) in the future, the amount of precipitation change, however, varied among GCMs. A drier climate was projected by MIROC5 versus a wetter climate by CNRM-CM5 (figures 4(c) and (d)), resulting in large discrepancies between GPP projections: by mid-century under RCP4.5, GPP projections with MIRCO5 (dry model) versus CNRM-CM5 (wet model) differed by as much as 36 g $cm^{-2}$ $yr^{-1}$ (figures 4(c) and (d); see detailed discussion in supplemental materials section 2). The sign of projected precipitation changes also varied by regions, in contrast to the warming trend across the state by all model simulations.

Climate change threatens California's annual rangelands, which are largely rainfall-dependent and therefore highly vulnerable to weather extremes (Macon *et al* 2016, Roche 2016). More extreme weather events and more frequent year-to-year weather swings in the future will lead to greater interannual rangeland productivity, potentially threatening the sustainability of forage supply and, ultimately, the resilience of ranches and rangelands to climate change. Other modeling approaches have similarly projected declines in productivity in various rangeland systems around the globe, with associated decreases in ecosystem goods and services, including livestock production (Boone *et al* 2018). The high degree of spatial variability in productivity impacts projected by our models means local, climate-informed decision-making will be increasingly critical to identifying adaptation strategies for mitigating climate risks.

This work can be leveraged to create near-real time rangeland productivity tracking and forecasting tools to support adaptive decision-making across California's extensive and highly variable rangelands. Future research and development will need to combine new data and emerging technologies with land management expertise to create locally-calibrated decision support systems. Working with land managers to co-develop decision-support

tools will ensure on-the-ground relevance to sustainability and resilience at local scales and, therefore, greatly increase manager adoption. Broader benefits potentially include producing locally-trusted tools and data to help inform policy and management guidance (e.g. drought and disaster early warning systems) at regional and national scales.

## 5. Conclusion

Climate change is expected to impact forage production across California's annual rangelands, threatening the economic viability and environmental sustainability of these highly valued systems. This study projected the degree to which GPP may respond to changes in different climatic variables by mid-century and end of century under RCP4.5 (intermediate emissions) and RCP8.5 (worst-case emissions) scenarios using remote sensing and machine learning techniques. Our machine learning-based analysis highlighted regional differences in GPP vulnerability to climate and provided insights on the intertwining and potentially counteracting effects of seasonal temperature and precipitation regimes. While total annual precipitation dominates the variations in annual GPP in drier ecoregions, changes in seasonal precipitation distribution affects the interannual GPP variability, especially in the wetter areas. We found that warmer winter season minimum air temperature promotes GPP for the majority of ecoregions; however, the maximum temperature during the GS reduced production in the CCR and NCICR. These results can inform rangeland management and conservation in the context of climate adaptation during an era of climate change.

## Data availability statement

The data that support the findings of this study are available upon reasonable request from the authors.

## Acknowledgments

This work was supported by the Russell L Rustici Rangeland and Cattle Research Endowment and partially by the California Strategic Growth Council under the Innovation Center for Advancing Ecosystem Climate Solutions.

## ORCID iDs

Han Liu https://orcid.org/0000-0003-3655-5561
Yufang Jin https://orcid.org/0000-0002-9049-9807
Leslie M Roche https://orcid.org/0000-0003-2954-8056
Randy A Dahlgren https://orcid.org/0000-0002-8961-875X

## References

Becchetti T *et al* 2016 Annual range forage production (University of California Agriculture and Natural Resources Publication) 8018 pp 1–12 (available at: http://anrcatalog.ucanr.edu/pdf/8018.pdf)

Boone R B, Conant R T, Sircely J, Thornton P K and Herrero M 2018 Climate change impacts on selected global rangeland ecosystem service *Glob. Change Biol.* **24** 1382–93

Briske D D, Karl J W, Herrick J E, Pyke D A, Karl J W, Herrick J E and Pyke D A 2017 Monitoring protocols: options, approaches, implementation, benefits *Rangeland systems* (Cham: Springer) pp 527–67

California Department of Food & Agriculture 2015 *2015 Crop Year Report* (Sacramento) (available at: www.cdfa.ca.gov/statistics/)

Chaplin-Kramer R and George M R 2013 Effects of climate change on range forage production in the San Francisco Bay area *PLoS One* **8** 1–11

Cleland D T, Freeouf J A, Keys J E, Nowacki G J, Carpenter C A and McNab W H 2007 Ecological subregions: sections and subsections for the conterminous United States *General Technical Report WO-76D* p 76

Dass P, Rawlins M A and Kimball J S 2016 Environmental controls on the increasing GPP of terrestrial environmental controls on the increasing GPP of terrestrial vegetation across Northern Eurasia vegetation across Northern Eurasia *BioScience* **13** 45–62

Devine S M, O'Geen A T, Larsen R E, Dahlke H E, Liu H, Jin Y and Dahlgren R A 2019 Microclimate–forage growth linkages across two strongly contrasting precipitation years in a mediterranean catchment *Ecohydrology* **12** 8

Elith J, Leathwick J and Hastie T 2008 A working guide to boosted regression trees *J. Anim. Ecol.* **77** 802–13

FRAP 2017 California's forests and rangelands: 2017 assessment. California department of forestry & fire protection (Sacramento, CA) (available at: https://frap.fire.ca.gov/media/3180/assessment2017.pdf)

Friedman J H 2001 Greedy function approximation: a gradient boosting machine *Ann. Stat.* **29** 1189–232

Friedman J H and Meulman J J 2003 Multiple additive regression trees with application in epidemiology *Stat Med.* **22** 1365–81

Guo Q, Hu Z, Li S, Yu G, Sun X, Zhang L and Zhao W 2015 Contrasting responses of gross primary productivity to precipitation events in a water-limited and a temperature-limited grassland ecosystem *Agric. For. Meteorol.* **214–215** 169–77

Guyon I, Weston J, Barnhill S and Vapnik V 2002 Gene selection for cancer classification using support vector machines *Mach. Learn.* **46** 389–422

Huang Y, Gerber S, Huang T and Lichstein J W 2016 Evaluating the drought response of CMIP5 models using global gross primary productivity, leaf area, precipitation, and soil moisture data *Glob. Biogeochem. Cycles* **30** 1827–46

Intergovernmental Panel on Climate Change (IPCC) 2013 *Climate Change 2013: The Physical Science Basis: Contribution of Working Group I to the Fifth Assessment Report of the Intergovernmental Panel on Climate Change* ed T Stocker *et al* (Cambridge: Cambridge University Press) (available at: www.ipcc.ch/report/ar5/)

Jin Y and Goulden M L 2014 Ecological consequences of variation in precipitation: separating short- versus long-term effects using satellite data *Glob. Ecol. Biogeogr.* **23** 358–70

Knapp A K, Beier C, Briske D D, Classen A T, Luo Y, Reichstein M and Weng E 2008 Consequences of more extreme precipitation regimes for terrestrial ecosystems *BioScience* **58** 811–21

Lee B, Kim N, Kim E S, Jang K, Kang M, Lim J H and Lee Y 2020 An artificial intelligence approach to predict gross primary productivity in the forests of South Korea using satellite remote sensing data *Forests* **11** 1000

Li S 2012 Monitoring of net primary production in California rangelands using landsat and MODIS satellite remote sensing *Nat. Res.* **3** 56–65

Liu H, Jin Y, Roche L M, O'Geen A T and Dahlgren R A 2021 Understanding spatial variability of forage production in California Grasslands: delineating climate, topography and soil controls *Environ. Res. Lett.* **16** 14–43

Lund HG 2007 Accounting for the world's rangelands *Rangelands* **29** 3–10

Macon D K, Barry S, Becchetti T, Davy J S, Doran M P, Finzel J A and Roche L M 2016 Coping with drought on California rangelands *Rangelands* **38** 222–8

Molnar C 2019 *Interpretable Machine Learning. A Guide for Making Black Box Models Explainable* (Victoria: Leanpub) (available at: https://christophm.github.io/interpretable-ml-book/)

Oliver J E 1980 Monthly precipitation distribution: a comparative index *Prof. Geogr.* **32** 300–9

Pierce D W, Kalansky J F and Cayan D R 2018 *Climate, Drought, and Sea Level Rise Scenarios for California's Fourth Climate Change Assessment* (La Jolla, CA: Scripps Institution of Oceanography, California Energy Commission)

Roche L M 2016 Adaptive rangeland decision-making and coping with drought *Sustainability* **8** 1334

Roche L M, Schohr T K, Derner J D, Lubell M N, Cutts B B, Kachergis E and Tate K W 2015 Sustaining working rangelands: insights from rancher decision making *Rangel. Ecol. Manage.* **68** 383–9

Running S, Mu Q and Zhao M 2019 MOD17A2H MODIS/terra gross primary productivity 8-Day L4 global 500m SIN grid V006 [data set] *NASA EOSDIS Land Processes DAAC* (https://doi.org/10.5067/MODIS/MOD17A2H.006)

Savtchenko A, Ouzounov D, Ahmad S, Acker J, Leptoukh G, Koziana J and Nickless D 2004 Terra and aqua modis products available from NASA GES DAAC *Adv. Space Res.* **34** 710–4

Shaw M R, Pendleton L, Cameron D R, Morris B, Bachelet D, Klausmeyer K and Roehrdanz P R 2011 The impact of climate change on California's ecosystem services *Clim. Change* **109** 465–84

Sloat L L, Gerber J S, Samberg L H, Smith W K, Herrero M, Ferreira L G and West P C 2018 Increasing importance of precipitation variability on global livestock grazing lands *Nat. Clim. Change* **8** 214–8

Stromberg M, Corbin J and D'Antonio C 2007 *California Grasslands: Ecology and Management* (Berkeley, CA: University of California Press)

Székely G J, Rizzo M L and Bakirov N K 2007 Measuring and testing dependence by correlation of distances *Ann. Stat.* **35** 2769–94

Thomson A M, Calvin K V, Smith S J, Kyle G P, Volke A, Patel P and Clarke L E 2011 $RCP_{4.5}$: a pathway for stabilization of radiative forcing by 2100 *Clim. Change* **109** 77

Thorne J H, Choe H, Boynton R M, Bjorkman J, Whitneyalbright W, Nydick K and Schwartz M W 2017 The impact of climate change uncertainty on California's vegetation and adaptation management *Ecosphere* **8** 12

Thornton P E, Thornton M M, Mayer B W, Wei Y, Devarakonda R, Vose R S and Cook R B 2016 *Daymet: Daily Surface Weather Data on a 1-km Grid for North America, Version 3* (ORNL Distributed Active Archive Center) (https://doi.org/10.3334/ORNLDAAC/1328)

U.S.Geological Survey 2016 *Explanations for the National Water Conditions* (available at: https://water.usgs.gov/nwc/explain_data.html) (Accessed 3 October 2022)

Wilson J D and Livingston B E 1932 Wilting and withering of grasses in greenhouse cultures as related to water-supplying power of the soil *Plant Physiol.* **7** 34

Wu C and Chen J M 2012 The use of precipitation intensity in estimating gross primary production in four Northern Grasslands *J. Arid Environ.* **82** 11–18

Xu L and Baldocchi D D 2004 Seasonal variation in carbon dioxide exchange over a mediterranean annual grassland in California *Agric. For. Meteorol.* **123** 79–96

Zhang Y *et al* 2016 Precipitation and carbon-water coupling jointly control the interannual variability of global land gross primary production *Sci. Rep.* **6** 39748

Zscheischler J, Reichstein M, Von Buttlar J, Mu M, Randerson J T and Mahecha M D 2014 Carbon cycle extremes during the 21st century in CMIP5 models: future evolution and attribution to climatic drivers *Geophys. Res. Lett.* **41** 8853–61